Translational Oncology

www.transonc.com

Volume 5 Number 6 December 2012 pp. 415–421 415

Multimodality Imaging of Tumor and Bone Response in a Mouse Model of Bony Metastasis[1]

Benjamin A. Hoff*, Komal Chughtai*, Yong Hyun Jeon*, Kenneth Kozloff†, Stefanie Galbán‡, Alnawaz Rehemtulla‡, Brian D. Ross* and Craig J. Galbán*

*Department of Radiology, University of Michigan, Ann Arbor, MI; †Department of Orthopaedic Surgery, University of Michigan, Ann Arbor, MI; ‡Department of Radiation Oncology, University of Michigan, Ann Arbor, MI

Abstract

Cancer drug development generally performs *in vivo* evaluation of treatment effects that have traditionally relied on detection of morphologic changes. The emergence of new targeted therapies, which may not result in gross morphologic changes, has spurred investigation into more specific imaging methods to quantify response, such as targeted fluorescent probes and bioluminescent cells. The present study investigated tissue response to docetaxel or zoledronic acid (ZA) in a mouse model of bony metastasis. Intratibial implantations of breast cancer cells (MDA-MB-231) were monitored throughout this study using several modalities: molecular resonance imaging (MRI) tumor volume and apparent diffusion coefficient (ADC), micro-computed tomography (μCT) bone volume, bioluminescence imaging (BLI) reporting cancer cell apoptosis, and fluorescence using Osteosense 800 and CatK 680-FAST. Docetaxel treatment resulted in tumor cell kill reflected by ADC and BLI increases and tumor volume reduction, with delayed bone recovery seen in μCT prefaced by increased osteoblastic activity (Osteosense 800). In contrast, the ZA treatment group produced similar values in MRI, BLI, and Osteosense 800 fluorescence imaging readouts when compared to controls. However, μCT bone volume increased significantly by the first week post-treatment and the CatK 680-FAST signal was slightly diminished by 4 weeks following ZA treatment. Multimodality imaging provides a more comprehensive tool for new drug evaluation and efficacy screening through identification of morphology as well as function and apoptotic signaling.

Translational Oncology (2012) 5, 415–421

Introduction

Bone metastases occur in more than 70% of advanced breast cancer patients with complications including bone fracture, pain, and spinal compression [1]. More than 250,000 patient deaths worldwide result from breast cancer, mainly attributed to metastatic disease [1]. Current treatments include systemic cytotoxic drugs, as well as bisphosphonates used for inhibition of bone loss, and are limited in their efficacy for combating bony metastasis [2,3]. Much recent research has been focused on targeted agents that disrupt specific closely involved signaling pathways in cancer. Effects of these treatments can be highly complex, which present challenges for the characterization of treatment response owing to the numerous mechanisms involved [4]. For example, recent studies in skeletal metastases have revealed important interactions between the tumor and its microenvironment [5–9]. It is well known that bone tissue harbors a latent pool of transforming growth factor–β (TGF-β) that when released by bone resorption propagates cancer growth in skeletal regions [2,10–12]. The discovery of this interdependency has spurred development of new targeted drugs to inhibit this cycle, resulting in a spectrum of agents targeting various stages of the cycle including TGF-β receptors in cancer cells, RANK in osteoclast precursors, cathepsin-K, and bisphosphonates for inhibiting

Address all correspondence to: Craig J. Galbán, PhD, Assistant Professor of Radiology, Center for Molecular Imaging, Biomedical Sciences Research Building, Room AC51, 109 Zina Pitcher Place, University of Michigan, Ann Arbor, MI 48109-2200. E-mail: cgalban@med.umich.edu

[1]We acknowledge the funding for this work from the National Institutes of Health (R01CA136892 and P50CA093990). B.D.R. and A.R. have financial interests in the underlying technology applying diffusion-weighted MRI for tumor treatment response monitoring.

Received 29 August 2012; Revised 12 November 2012; Accepted 12 November 2012

1944-7124/12 DOI 10.1593/tlo.12298

osteoclast activity [11]. Conventional anatomic imaging and histologic techniques for quantifying response to therapy are insufficient for capturing the time-dependent interactions and targeted mechanisms of this complex system. Conventional approaches to monitoring cancer response to therapy are limited, with the most prevalent being changes in tumor volume followed by quantitative measurements of tissue perfusion and diffusion. Because of the unconventional action these agents have on metastatic breast cancer to the bone, a more comprehensive assessment of tumor biology and response to intervention would provide investigators developing new targeted agents with improved insights into the complicated interrelationships of the signaling pathways and their role in tumor growth and cell death.

In this study, a multimodality approach to imaging treatment response was undertaken in an effort to more fully delineate the underlying biologic responses to bisphosphonate and taxane treatment using a mouse model of established breast cancer metastasis to the bone. Molecular resonance imaging (MRI) was used to monitor tumor soft tissue volumetric response and cellularity; micro-computed tomography (μCT) was used to monitor bone characteristics; bioluminescence imaging (BLI) was used to monitor apoptosis by measuring caspase-3–linked activation; and fluorescent probes targeting bone mineralization and cathepsin-K activity were used to provide information related to bone remodeling activity. Noninvasive imaging provided for longitudinal assessment of differential treatment effects on bone and tumor following administration with docetaxel and zoledronic acid (ZA). Imaging readouts were able to follow signatures unique to response of tumor and bone, revealing the capability of applying imaging modalities to "unmix" the complex biologic responses to individual therapies, thus providing opportunities for assessing more complex treatments targeting mixed osteoblastic and osteoclastic phenotypes. Overall, the application of multiple imaging approaches described herein provide a more comprehensive and robust process than any single-modality approach for new drug evaluation and efficacy screening through delineation of treatment effects on tumor and bone morphology as well as functional and signaling pathways.

Materials and Methods

Animal Tumor Model

Female severe combined immunodeficiency mice were subject to intratibial implantation of MDA-MB-231 breast cancer subline 1833 cells transfected with a luciferase reporter on caspase-3 (Figure 1, PPOP [13], Promega Corporation, Madison, WI) in the right leg with 10^5 cells in 5 μl of serum-free medium suspension. Briefly, mice were anesthetized with an intraperitoneal injection of ketamine and then leg hair was removed using Nair. An empty 0.5-cm^3 insulin syringe was used to bore a hole down into the tibial marrow space through the tibial plateau through which a Hamilton syringe was then used to insert the cell suspension. A sham injection of media alone was performed on the left leg as a surgical control.

Treatments

Once tumor size reached a volume of 10 to 20 mm^3 (as measured by MRI), mice were separated into treatment groups of ZA (n = 16), docetaxel (n = 7), or control (n = 17). ZA treatment was administered subcutaneously as 100 μg in 100 μl of phosphate-buffered saline (PBS, 5 mg/kg) per mouse twice weekly for four treatments, docetaxel was administered intravenously at a dose of 20 mg/kg weekly for three cycles, and control mice were administered PBS with the same schedule as ZA. Control animals treated with 10% ethanol were also considered but were found not to differ from PBS controls so are not shown.

Imaging and Analysis

Molecular Resonance Imaging. MRI was performed using a 7-T, 16-cm horizontal bore DirectDrive System (Agilent Technologies, Palo Alto, CA) with a quadrature mouse head coil (m2m Imaging Corp, Cleveland, OH). Images of the tumor-bearing leg were acquired twice weekly starting from the day before treatment initiation. Diffusion-weighted images were acquired using a spin-echo sequence with navigator echo motion correction and gradient waveforms sensitive to isotropic diffusion [14] using the following parameters: repetition time/echo time = 4000/37 ms, field of view = 20 × 20 mm, matrix size = 128 × 64, slice thickness = 0.5 mm, slice number = 25, and b values (diffusion weighting) of 120 and 1200 s/mm^2. Following image acquisition, data that included manually drawing volumes of interest on the high diffusion-weighted image to compute tumor volumes and diffusion values were stored for analysis. Tumor volumes and apparent diffusion coefficient (ADC) values were quantified over time to monitor tumor burden and cellularity, respectively.

Micro-computed Tomography. μCT imaging was performed weekly starting from the day before treatment initiation using a Siemens Inveon System with the following parameters: 80 kVp, 500 μA, 300-ms exposure, 501 projections over 360 degrees, and 49.2-mm field of view (56-μm voxel size). Volumes of interest were drawn over the tibia from the tibia-fibula junction to the tibial plateau, measuring mean bone volume and mineral density throughout the study to monitor bone resorption.

Bioluminescence Imaging. For imaging of the PPOP-transfected cells, mice were injected with 200 mg/kg luciferin (Promega), and up to five mice were imaged in a single BLI scan, acquiring a series of images to find the total photon peak flux over a whole-leg region of interest (ROI) for each animal. Images were acquired on the day of treatment initiation and days 7, 10, 14, 21, and 28 afterward. BLI data

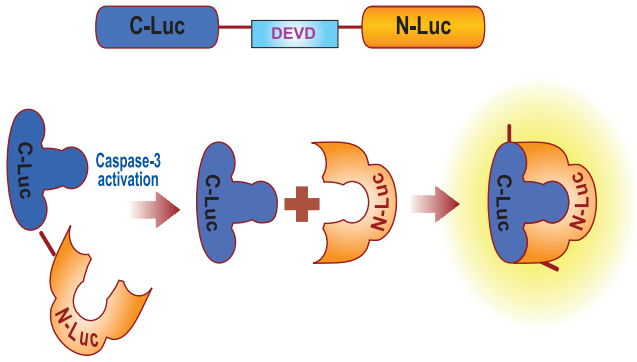

Figure 1. Diagram of the split luciferase construct used in this model. A split-luciferase complex is expressed in the cells with a DEVD sequence between the N-Luc and C-Luc domains, keeping the enzyme inactive through steric hindrance. When caspase-3 is expressed in the cell, signaling the cell to begin apoptotic events, active caspase-3 cleaves the DEVD sequence from the rest of the enzyme. Active luciferase then metabolizes luciferin substrate and emits light.

were quantified as total photon peak flux normalized by tumor volume as measured by MRI.

Fluorescence Imaging. Fluorescence images were acquired on an IVIS Spectrum System (PerkinElmer, Inc, Walther, MA) every other week using the two probes: Osteosense 800 and CatK 680-FAST (PerkinElmer, Inc). Fluorescent probes were injected intravenously 24 hours before imaging, and hair was removed from the hind legs the same day using Nair lotion. The following optical filter sets were used for each acquisition:

Emission (nm)	Emission (nm)		
430	500	580	640
675	720	740	760
745	800	820	840

After acquisition, images were spectrally unmixed using Living Image software (Caliper Life Sciences) to separate the two probe signals from each other and autofluorescence. ROIs with the same area were placed over both the left and right legs and signal was measured as the ratio (right/left) of mean radiant efficiency to account for variation in fluorophore injection, physiology, and possible accumulation of fluorescent agent because of the high frequency of imaging.

Statistics. A Student's *t* test was used to compare means between groups at each time point. Results with $P < .05$ were considered statistically significant. All plots represent mean ± SEM.

Results

MRI was performed to monitor tumor volume and water diffusivity (ADC) twice weekly throughout the study (Figure 2). This modality was able to detect a significant retardation of tumor growth (Figure 2*A*) in the docetaxel-treated group by day 6 compared to the control and ZA-treated groups, which was followed by tumor shrinkage with no recovery within the study time frame. In addition, ADC values of the docetaxel-treated group were found to significantly increase by day 6 (Figure 2*B*), indicating that significant tumor cell death in the docetaxel group had occurred following treatment initiation. The ZA group however showed no significant difference from control tumor ADC values over the duration of the study although both trended downward, indicating that increasing density or packing of tumor cells occurred during the multifold volumetric increase in tumor size. Representative ADC map overlays for each of the animal groups (Figure 2*C*) revealed consistently low ADC values in the control and ZA groups, whereas localized regions in the docetaxel-treated tumors became elevated before and during tumor shrinkage.

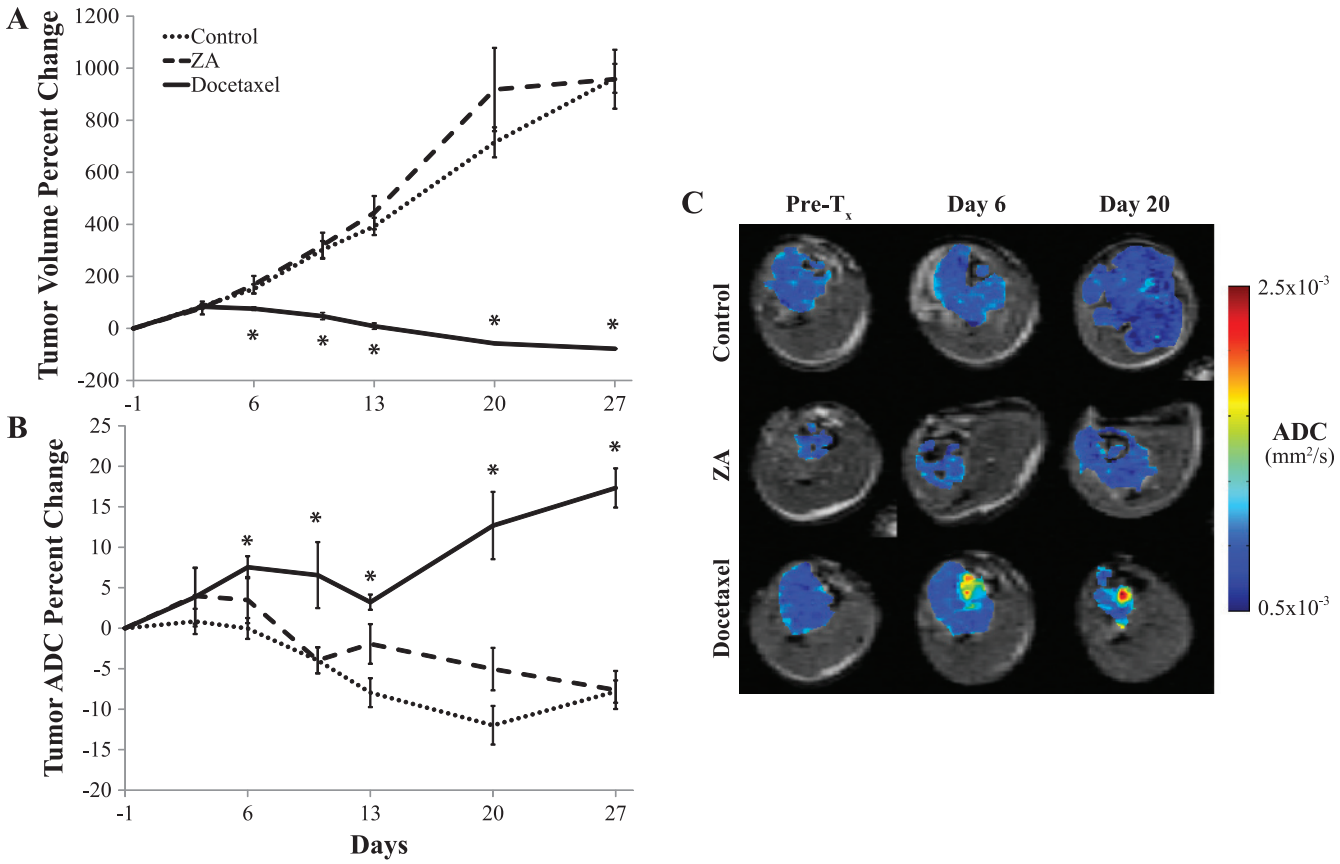

Figure 2. (A) Plots of percent change in tumor volume for each group show significant cell kill in the docetaxel group but no significant effect in the ZA group. (B) Plots of percent change in tumor ADC show elevated values in the docetaxel group after day 6 but no significant change in the ZA group. (C) Representative ADC overlays show isolated areas of increased ADC in the docetaxel group (red) as well as a dramatic decrease in tumor volume seen at day 20. Asterisk indicates a significant difference from the control group ($P < .05$).

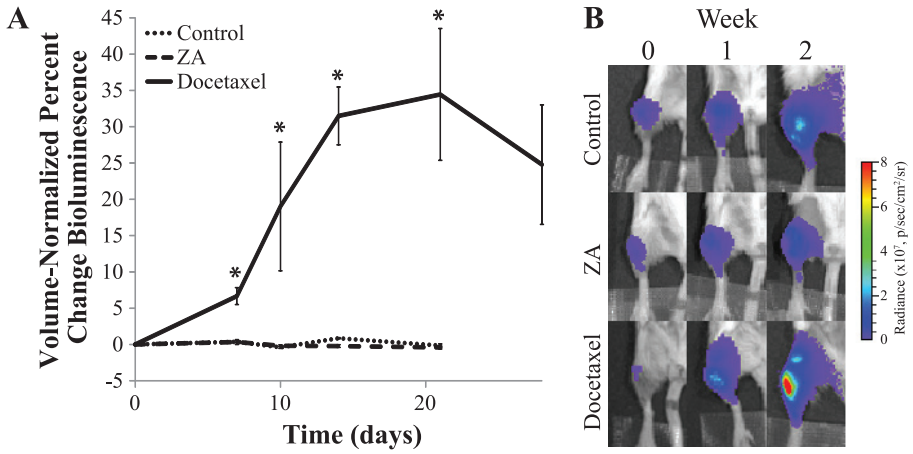

Figure 3. (A) Plots of overall luminescence of the tumor-bearing leg over time. Values are shown as the percent change of total photon flux (over a fixed-area ROI) normalized by tumor volume (as measured by MRI). (B) Representative radiance overlays show increased caspase-3 activity in the docetaxel group and minimal change in the control and ZA groups. Asterisk indicates a significant difference from the control group ($P < .05$).

BLI of the PPOP reporter (Figure 3) revealed an increase in caspase-3 activity in the docetaxel group within 1 week of treatment, which remained elevated until the end of the study. Control and ZA groups both remained at baseline levels throughout the study, indicating that no significant apoptotic activation occurred. Representative bioluminescence images for each of the three groups (Figure 3*B*) showed that a stable low level of photons were emitted from the tumor sites in the control and ZA groups over time, whereas an increase in photon counts in the docetaxel group occurred (Figure 3*B*).

To monitor bone changes with therapy, μCT imaging was performed weekly and bone volume within the proximal tibia was quantified over the 4-week duration of the study (Figure 4*A*). Within 1 week of treatment with ZA, a significant increase in bone volume was detected, which remained elevated throughout the study. The docetaxel group showed a delayed bone response, with a significant increase in bone volume observed at week 3. Control mice were found to have a stable total bone volume until week 3 followed by significant bone degradation. Representative images (Figure 4*B*) show progressive bone degradation in the control group throughout the study, whereas the ZA mouse's bone seemed to have stabilized even though growth of the soft tissue tumor appears to be fracturing the bone in certain weakened locations. Docetaxel-treated mice showed delayed bone response, with significant recovery by week 4.

Fluorescence imaging (FLI) was performed to obtain a more functional assessment of bone remodeling, with Osteosense 800 indicating the extent of bone reformation and activatable CatK 680-FAST indicating the level of osteolytic activity. The plots in Figure 5 show that significant bone remodeling changes occurred at weeks 2 and 4

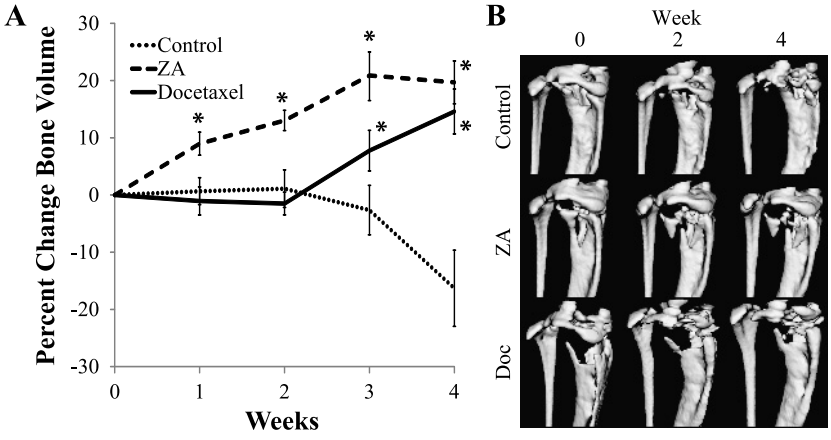

Figure 4. (A) Plots of tumor-bearing bone volume from μCT. The control group remained stable over the first 2 weeks followed by a sharp decline beginning at week 3. An increase in the ZA group was seen by the first week and remained elevated, whereas a significant increase was not seen in the docetaxel group until week 3 and almost reached the ZA group by week 4. (B) Representative image isosurfaces in the three groups. Controls presented successive bone degradation throughout the study. ZA-treated animals showed minimal changes in bone structure, with only fracturing caused by tumor growth. Docetaxel-treated animals showed some initial degradation through week 2 followed by recovery seen by week 4. Asterisk indicates a significant difference from the control group ($P < .05$).

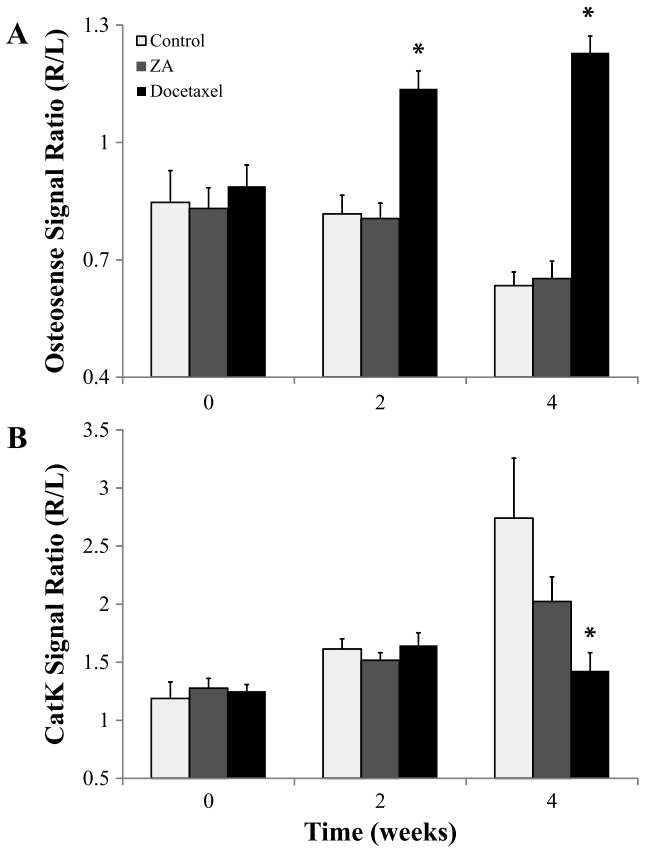

Figure 5. Bar plots of fluorescent signals in the tumor-bearing leg from (A) Osteosense 800 and (B) CatK 680-FAST are presented as values normalized by the non-tumor–bearing leg. The ZA group showed no significant difference from controls with either fluorescent probe, but the docetaxel group showed significant increases in Osteosense 800 uptake (A, black bar) on weeks 2 and 4 and a significant drop in CatK 680-FAST signal (B, black bar) on week 4. Asterisk indicates a significant difference from the control group ($P < .05$).

in the docetaxel-treated group, whereas there was no significant change detected in the ZA or control group. The progressive increase in relative Osteosense 800 signal for the docetaxel group indicated that there was a significant amount of bone reformation by week 2, earlier than the CT-evaluated bone response, which was maintained until the end of the study. CatK 680-FAST signal also showed a significant reduction compared to controls in the docetaxel group by week 4. The control group showed a progressive increase in CatK 680-FAST signal, indicating tumor growth and increased activation of osteoclasts. The ZA group did show attenuated CatK 680-FAST activation, which would be consistent with the reduction in bone loss seen by CT but was not found to be significant compared to controls.

Discussion

The goal of this study was to investigate the use of multiple imaging biomarker readouts to interrogate interrelated biologic responses involved in the treatment of bony cancers in an effort to provide a more complete understanding of the overall biologic effects *in vivo*. Current preclinical studies rely heavily on histologic analysis, where a number of subjects must be sacrificed at each time point in the study to assess tissue responses. However, with the increasing variety of noninvasive imaging tools available, successful longitudinal studies may be strategically planned to reduce total subject numbers while maximizing the amount of information that can be extracted from each subject. This method will be increasingly useful for the evaluation of new therapies that may have multiple targets and require simultaneous monitoring of multiple processes. In the case of metastatic bone disease, assessments of treatments that affect both the soft tissue tumor and mineralized bone are important because of the known biologic interactions between the two as well as clinical implications in avoiding skeletal-related events, e.g., fracture. As newer treatments may not be directly involved in causing cell death or other conventionally quantifiable tissue responses, optical imaging techniques can be applied to assess treatment-related alterations in multiple cellular processes *in vivo* simultaneously and longitudinally over time. Optical readouts of treatment effects can be obtained from activatable and targeted FLI probes as well as genetically engineered tumor cells whose molecular signaling events can be monitored noninvasively by BLI, which compliment more traditional imaging techniques such as MRI and CT.

The use of MRI and CT for evaluation of soft tissues and bone, respectively, has long been established. Quantification of tissue response to therapy using these imaging modalities has classically been through morphologic changes such as tumor or bone volume, with the more recent development of functional imaging techniques such as diffusion MRI [14–19] and perfusion measurements acquired by MRI or CT [20–23]. The recent trend in therapeutic research, however, is toward modification of specific cellular signaling pathways using targeted agents that may not have such drastic morphologic effects. With these new agents, conventional imaging approaches may not have enough sensitivity or specificity to determine treatment effects *in vivo*. In this study, we have presented a multimodality approach to evaluate treatment response using readouts obtained through pathway-specific optical imaging techniques backed by conventional μCT and MRI, which are clinically relevant modalities that provide more general information on morphology and gross tissue characteristics. We evaluated two treatments representing the extremes of either tumor-specific or bone-specific therapies to more easily illustrate the separate effects of these agents on the complex tumor-stromal interaction. Tumor ADC response has been tested on a broad range of cases and shown to correlate with cell death and often preclude any detectable change in tumor volume [14–19], however, ADC alone cannot determine the mechanism of cell death. The inclusion of caspase-3–coupled bioluminescence in this case provides the link between treatment and the specific mechanism. The significant increase in normalized BLI signal in the docetaxel group over the controls indicates that, through caspase-3 signaling, cells are undergoing apoptotic cell death. Tumor ADC values did not show a significant difference between docetaxel and control groups before tumor volume. This is attributed to MDA-MB-231 cell lines aggressiveness and high sensitivity to docetaxel.

FLI results using our two probes shed further light on the bone remodeling processes resulting from the tumor and treatments. Where μCT provides a high-resolution view of the current state of the bone, FLI is sensitive to the balance between processes of bone formation and erosion. The significant increase in the Osteosense 800 signal and dampening of the CatK 680-FAST signal for the docetaxel group indicates that induction of tumor cell kill and subsequent reduction in tumor burden has inhibited the tumor-stromal interaction, i.e., "vicious cycle" [2], and shifted the balance of osteoblastic and osteolytic activities toward recovery. Tumor apoptosis following effective

treatment by docetaxel led to a reduction in osteoclast recruitment and subsequently fewer cathepsin-K–expressing cells in that region, where even MDA-MB-231 cells have been shown to express cathepsin-K [24]. In addition, the disruption of the tumor-stromal interaction allowed for an up-regulation of osteoblastic activity as evidenced by an increase in Osteosense 800 signaling. As expected, treatment with ZA had no effect on tumor burden, suggesting that tumor signaling to the stroma was undisrupted during treatment. In contrast to what we observed using docetaxel, ZA did not significantly affect the Osteosense 800 signal ratio that would have been presumed based on the μCT results where an increase in bone volume was observed. Although not significant, the CatK 680-FAST signaling was slightly reduced in the ZA group when compared to controls. This may indicate that ZA protects the bone by reducing the extent of osteolytic activity, in essence shifting total bone turnover in the presence of a tumor from bone erosion to bone formation [14–23,25–30].

When using a strategy for assessing the efficacy of a therapy using a multimodality imaging approach, it is important to take into account the limitations of the desired imaging modalities when planning a study. MRI and CT are both able to capture relatively high-resolution images, providing easily quantified volume and ADC measurements, as well as being translated to the clinic. These two modalities, however, do not provide any information about the signals or mechanics of the biologic system. In contrast, the optical techniques described here provide detailed information on biologic processes and signaling but are confined to preclinical use. BLI and FLI are known to present challenging hurdles for *in vivo* quantification, such as assumptions of light attenuation and scattering through tissues, limited spatial resolution, and error in the injected probe/substrate. In the presented work, the fluorescent signal in the tumor-bearing leg was normalized by the signal in the sham leg to account for variability of injection and heightened Osteosense 800 signal in the growth plates. The poor image resolution of FLI complicates matters further by having to contend with spillover signal from the growth plates. Nevertheless, with an established imaging protocol for acquiring data, care in image postprocessing, and an appropriate model, these limitations can be overcome to provide a full picture of the effects of a therapeutic agent on a tumor-stromal microenvironment.

Overall, the experiments presented here demonstrate the use of multimodality imaging techniques for detection and quantification of multiple interrelated biologic processes affected by therapeutic intervention in a model of metastatic bone disease. Although the treatments were selected on the basis of their current clinical relevance and their targeted effects on bone or tumor cells, this generalizable approach is anticipated to be useful in future studies identifying responses to experimental agents by obtaining a more complete understanding of the signaling pathways affected. These and other cancer cell lines have already been successfully engineered to express luciferase linked to cellular signals such as AKT, TGF-β, c-MET, epidermal growth factor receptor (EGFR), and others [26,28,29,31,32]. In addition, a wide variety of *in vivo* fluorescent agents (activatable and targeted) are already available, for imaging of many diseases. Selection of optical imaging agents, cell lines, and other imaging modalities, such as permeability MRI for measuring tumor vasculature, requires careful evaluation of which experimental readouts provide the most relevant information for assessing the efficacy of a novel agent as a single or combination therapy.

In summary, experimental therapeutic agents have traditionally relied on anatomic and functional imaging readouts of treatment response. With the emergence of optical imaging approaches including reporter cell–based constructs and activatable and targeted exogenously administered probes, the interdependence of treatment responses due to complex tumor-host interactions can be more fully delineated. BLI and FLI *in vivo* methods may be tailored to most diseases and treatment interventions and are complementary to MRI and CT imaging readouts. The use of a multimodality imaging strategy is anticipated to provide the pharmaceutical industry with cost-effective and efficient options for furthering overall drug development strategies.

References

[1] Coleman RE (2001). Metastatic bone disease: clinical features, pathophysiology and treatment strategies. *Cancer Treat Rev* **27**, 165–176.

[2] Mundy GR (2002). Metastasis to bone: causes, consequences and therapeutic opportunities. *Nat Rev Cancer* **2**, 584–593.

[3] Tkaczuk KH (2009). Review of the contemporary cytotoxic and biologic combinations available for the treatment of metastatic breast cancer. *Clin Ther* **31**(pt 2), 2273–2289.

[4] Korpal M, Yan J, Lu X, Xu S, Lerit DA, and Kang Y (2009). Imaging transforming growth factor-β signaling dynamics and therapeutic response in breast cancer bone metastasis. *Nat Med* **15**, 960–966.

[5] Casimiro S, Guise TA, and Chirgwin J (2009). The critical role of the bone microenvironment in cancer metastases. *Mol Cell Endocrinol* **310**, 71–81.

[6] Guise TA (2002). The vicious cycle of bone metastases. *J Musculoskelet Neuronal Interact* **2**, 570–572.

[7] Joyce JA and Pollard JW (2009). Microenvironmental regulation of metastasis. *Nat Rev Cancer* **9**, 239–252.

[8] Ooi LL, Zheng Y, Stalgis-Bilinski K, and Dunstan CR (2011). The bone remodeling environment is a factor in breast cancer bone metastasis. *Bone* **48**, 66–70.

[9] Zheng Y, Zhou H, Brennan K, Blair JM, Modzelewski JR, Seibel MJ, and Dunstan CR (2007). Inhibition of bone resorption, rather than direct cytotoxicity, mediates the anti-tumour actions of ibandronate and osteoprotegerin in a murine model of breast cancer bone metastasis. *Bone* **40**, 471–478.

[10] Dunn LK, Mohammad KS, Fournier PG, McKenna CR, Davis HW, Niewolna M, Peng XH, Chirgwin JM, and Guise TA (2009). Hypoxia and TGF-β drive breast cancer bone metastases through parallel signaling pathways in tumor cells and the bone microenvironment. *PLoS One* **4**, e6896.

[11] Onishi T, Hayashi N, Theriault RL, Hortobagyi GN, and Ueno NT (2010). Future directions of bone-targeted therapy for metastatic breast cancer. *Nat Rev Clin Oncol* **7**, 641–651.

[12] Rose AA and Siegel PM (2010). Emerging therapeutic targets in breast cancer bone metastasis. *Future Oncol* **6**, 55–74.

[13] Galbán S, Jeon YH, Sharkey LM, Hoff BA, Galbán CJ, Ross BD, and Rehemtulla A (2012). A genetically engineered mouse for imaging of apoptosis in a tissue specific manner. In *Proceedings of the 103rd AACR Annual Meeting, 2012 March 31–April 4.* Chicago, IL. Poster session presented at: AACR 2012.

[14] Moffat BA, Hall DE, Stojanovska J, McConville PJ, Moody JB, Chenevert TL, Rehemtulla A, and Ross BD (2004). Diffusion imaging for evaluation of tumor therapies in preclinical animal models. *MAGMA* **17**, 249–259.

[15] Chenevert TL, Stegman LD, Taylor JM, Robertson PL, Greenberg HS, Rehemtulla A, and Ross BD (2000). Diffusion magnetic resonance imaging: an early surrogate marker of therapeutic efficacy in brain tumors. *J Natl Cancer Inst* **92**, 2029–2036.

[16] Galbán CJ, Bhojani MS, Lee KC, Meyer CR, Van Dort ME, Kuszpit KK, Koeppe RA, Ranga R, Moffat BA, Johnson TD, et al. (2010). Evaluation of treatment-associated inflammatory response on diffusion-weighted magnetic resonance imaging and 2-[^{18}F]-fluoro-2-deoxy-D-glucose-positron emission tomography imaging biomarkers. *Clin Cancer Res* **16**, 1542–1552.

[17] Hamstra DA, Rehemtulla A, and Ross BD (2007). Diffusion magnetic resonance imaging: a biomarker for treatment response in oncology. *J Clin Oncol* **25**, 4104–4109.

[18] Ross BD, Moffat BA, Lawrence TS, Mukherji SK, Gebarski SS, Quint DJ, Johnson TD, Junck L, Robertson PL, Muraszko KM, et al. (2003). Evaluation of cancer therapy using diffusion magnetic resonance imaging. *Mol Cancer Ther* **2**, 581–587.

[19] Hoff BA, Chenevert TL, Bhojani MS, Kwee TC, Rehemtulla A, Le Bihan D, Ross BD, and Galbán CJ (2010). Assessment of multiexponential diffusion

features as MRI cancer therapy response metrics. *Magn Reson Med* **64**, 1499–1509.

[20] Bauerle T, Bartling S, Berger M, Schmitt-Graff A, Hilbig H, Kauczor HU, Delorme S, and Kiessling F (2010). Imaging anti-angiogenic treatment response with DCE-VCT, DCE-MRI and DWI in an animal model of breast cancer bone metastasis. *Eur J Radiol* **73**, 280–287.

[21] Walker-Samuel S, Leach MO, and Collins DJ (2006). Evaluation of response to treatment using DCE-MRI: the relationship between initial area under the gadolinium curve (IAUGC) and quantitative pharmacokinetic analysis. *Phys Med Biol* **51**, 3593–3602.

[22] Yankeelov TE, Lepage M, Chakravarthy A, Broome EE, Niermann KJ, Kelley MC, Meszoely I, Mayer IA, Herman CR, McManus K, et al. (2007). Integration of quantitative DCE-MRI and ADC mapping to monitor treatment response in human breast cancer: initial results. *Magn Reson Imaging* **25**, 1–13.

[23] Hoff BA, Bhojani MS, Rudge J, Chenevert TL, Meyer CR, Galbán S, Johnson TD, Leopold JS, Rehemtulla A, Ross BD, et al. (2011). DCE and DW-MRI monitoring of vascular disruption following VEGF-Trap treatment of a rat glioma model. *NMR Biomed* **25**, 935–942.

[24] Tomita A, Kasaoka T, Inui T, Toyoshima M, Nishiyama H, Saiki H, Iguchi H, and Nakajima M (2008). Human breast adenocarcinoma (MDA-231) and human lung squamous cell carcinoma (Hara) do not have the ability to cause bone resorption by themselves during the establishment of bone metastasis. *Clin Exp Metastasis* **25**, 437–444.

[25] Xie BW, Mol IM, Keereweer S, van Beek ER, Que I, Snoeks TJ, Chan A, Kaijzel EL, and Lowik CW (2012). Dual-wavelength imaging of tumor progression by activatable and targeting near-infrared fluorescent probes in a bioluminescent breast cancer model. *PLoS One* **7**, e31875.

[26] Bhojani MS, Nyati MK, Zhao L, Normolle DP, Ross BD, Lawrence TS, and Rehemtulla A (2011). Molecular imaging of Akt enables early prediction of response to molecular targeted therapy. *Transl Oncol* **4**, 122–125.

[27] Coppola JM, Ross BD, and Rehemtulla A (2008). Noninvasive imaging of apoptosis and its application in cancer therapeutics. *Clin Cancer Res* **14**, 2492–2501.

[28] Nyati S, Schinske K, Ray D, Nyati M, Ross BD, and Rehemtulla A (2011). Molecular imaging of TGFβ-induced Smad2/3 phosphorylation reveals a role for receptor tyrosine kinases in modulating TGFβ signaling. *Clin Cancer Res* **17**, 7424–7439.

[29] Zhang L, Virani S, Zhang Y, Bhojani MS, Burgess TL, Coxon A, Galbán CJ, Ross BD, and Rehemtulla A (2011). Molecular imaging of c-Met tyrosine kinase activity. *Anal Biochem* **412**, 1–8.

[30] Galbán CJ, Galbán S, Van Dort ME, Luker GD, Bhojani MS, Rehemtulla A, and Ross BD (2010). Applications of molecular imaging. *Prog Mol Biol Transl Sci* **95**, 237–298.

[31] Khan AP, Contessa JN, Nyati MK, Ross BD, and Rehemtulla A (2011). Molecular imaging of epidermal growth factor receptor kinase activity. *Anal Biochem* **417**, 57–64.

[32] Zhang L, Lee KC, Bhojani MS, Khan AP, Shilman A, Holland EC, Ross BD, and Rehemtulla A (2007). Molecular imaging of Akt kinase activity. *Nat Med* **13**, 1114–1119.